Two examples of nanostructured gold surfaces as biosensors. Surface-enhanced chemiluminescence and double detection by surface plasmon resonance and luminescence

Grégory Barbillon[1], Meigui Ou[2], Anne-Charlotte Faure[1], Christophe Marquette[3], Jean-Louis Bijeon[4], Olivier Tillement[1], Stéphane Roux[1] and Pascal Perriat[2]

[1] Université de Lyon, Université Lyon 1, CNRS UMR 5620, Laboratoire de Physico-Chimie des Matériaux Luminescents (LPCML), Domaine scientifique de La Doua, Bât Kastler, 10 rue André Marie Ampère 69622 Villeurbanne Cédex, France
[2] Matériaux, Ingénierie et Sciences (MATEIS), CNRS UMR 5510, Université de Lyon, INSA-Lyon, Domaine scientifique de La Doua, 7 avenue Jean Capelle 69621 Villeurbanne Cédex, France
[3] Laboratoire de Génie Enzymatique et Biomoléculaire, UMR 5246 CNRS-ICBMS, Université de Lyon, Université Lyon 1, 69622 Villeurbanne Cédex, France
[4] Institut Charles Delaunay, CNRS FRE 2848, Laboratoire de Nanotechnologie et d'Instrumentation Optique (LNIO), Université de Technologie de Troyes, 12 rue Marie Curie BP 2060 10010 Troyes Cédex, France
E-mail : Pascal.Perriat@insa-lyon.fr

Abstract

In this paper, we present a review of our activities in the field of gold biosensors. Nanostructured gold surfaces can be used in biology for their plasmonic and/or catalytic properties. In a first part, we show how the gold plasmonic properties allow the detection of the biotin-streptavidin binding by two types of techniques: extinction spectroscopy and also luminescence spectroscopy when the probe (here the streptavidin) is labelled by polysiloxane particles encapsulating fluorophores. In a second part, we demonstrate that the catalytical properties of gold corrugated surfaces can significantly enhance the chemiluminescence of luminol brought at vicinity. We found that the surface-enhancement induced by gold is two times of magnitude greater than that induced by silver.

1 Introduction

Since a few decades, various groups of researchers work on nanostructured gold surfaces applied to biology as biosensors. The development of biosensors is an extremely significant problem for the diagnosis and monitoring diseases, proteomics and the environmental detection of biological agents [1]. The first studied biosensors were Surface Plasmon Resonance (SPR) sensors. The potential of SPR biosensors was recognized in 1980s by Liedberg *et al.* [2], who were able to detect immunoglobulin antibodies by observing the change in critical angle when the antibodies bind selectively on an Au film. Since their original discovery, SPR sensors changes have been used in refractive-index-based sensing to detect analyte binding at or near a metal surface. Moreover, the SPR sensors has been used to monitor a broad range of analyte-surface binding interactions as the adsorption of small molecules [3,4,5], protein adsorption on self-assembled monolayers [6,7], DNA hybridisation [8] and protein-DNA interactions [9]. Then, different groups were interested in the Localized Surface Plasmon Resonance (LSPR) sensors, which induce a local refractive index changes after adsorption of biological molecules [10, 11, 12, 13, 14, 15, 16, 17]. The differences between the SPR and the LSPR sensors are respectively their refractive index sensitivities 2.10^6 nm/RIU (Refractive Index Unit) [3] and 2.10^2 nm/RIU [10] and respectively their evanescent electric field decay lengths l_d = 200-300 nm [3] and l_d = 5-30 nm [10,11,12]. However, the two types of sensors are very competitive in their sensitivities, because the two characteristics are compensated. The LSPR nanosensors require no temperature control (low refractive index sensitivity) compared to the SPR nanosensors where a control is necessary because of the large refractive index sensitivity.

Another technique, which is used for the biodetection, is the SERS (Surface Enhanced Raman Scattering). Two mechanisms are known to contribute to SERS: an increase of the local electromagnetic field, *i.e.* a plasmonic effect [18]

and an electronic interaction between the metal and adsorbate, that is a "chemical effect" [19]. This phenomenon whereby specific molecules at or near a roughed metal nanosurface undergo a big increase in the intensity of the observed inelastically scattered light lead, since the 1980s, to an increasing number of biological applications [20] like the *in vivo* molecular imaging of cancer [21] or surface-enhanced Raman spectroscopy of DOPA-containing peptides [22]. Following the development of SERS, other surface-enhanced (SE) phenomena have been studied in the last decades like SE fluorescence (SEF) but SE chemiluminescence (SECL) is the last that has been evidenced. It has been reported for luminol near gold particles [23] or corrugated films [24]. Even if the mechanisms responsible for SECL are still controversial, a series of papers (including ours) prove that they could be, contrarily to SEF, related to a catalytic effect rather than to a plasmonic one. This observation is consistent with the general observation that, even if bulk gold is chemically inert, gold particles turns out to be surprisingly active for many reactions [25, 26, 27]. In this review, we will focus two works developed by our team and we will present:

- a promising aspect of gold nanostructures brought by plasmonic properties *i.e.* the possibility of multimodal detection using LSPR of the substrate and the luminescence of labelling nanoparticles
- a promising aspect of these structures induced by their catalytic properties *i.e.* SECL

2 Description of the gold substrates used

2.1 Brief review of the techniques used in literature

A certain number of fabrication techniques allow to controllably and reproducibly elaborate nanostructured gold substrates for biology among which electron beam lithography, nanosphere lithography and pulsed laser deposition (PLD).

2.2 Structuration of gold surfaces by Lithographic techniques

This class of techniques realizes substrate-bound nanostructure fabrication. The most known technique is electron beam lithography (EBL). It permits to serially obtain patterns with controlled shape, size, and interparticle spacing

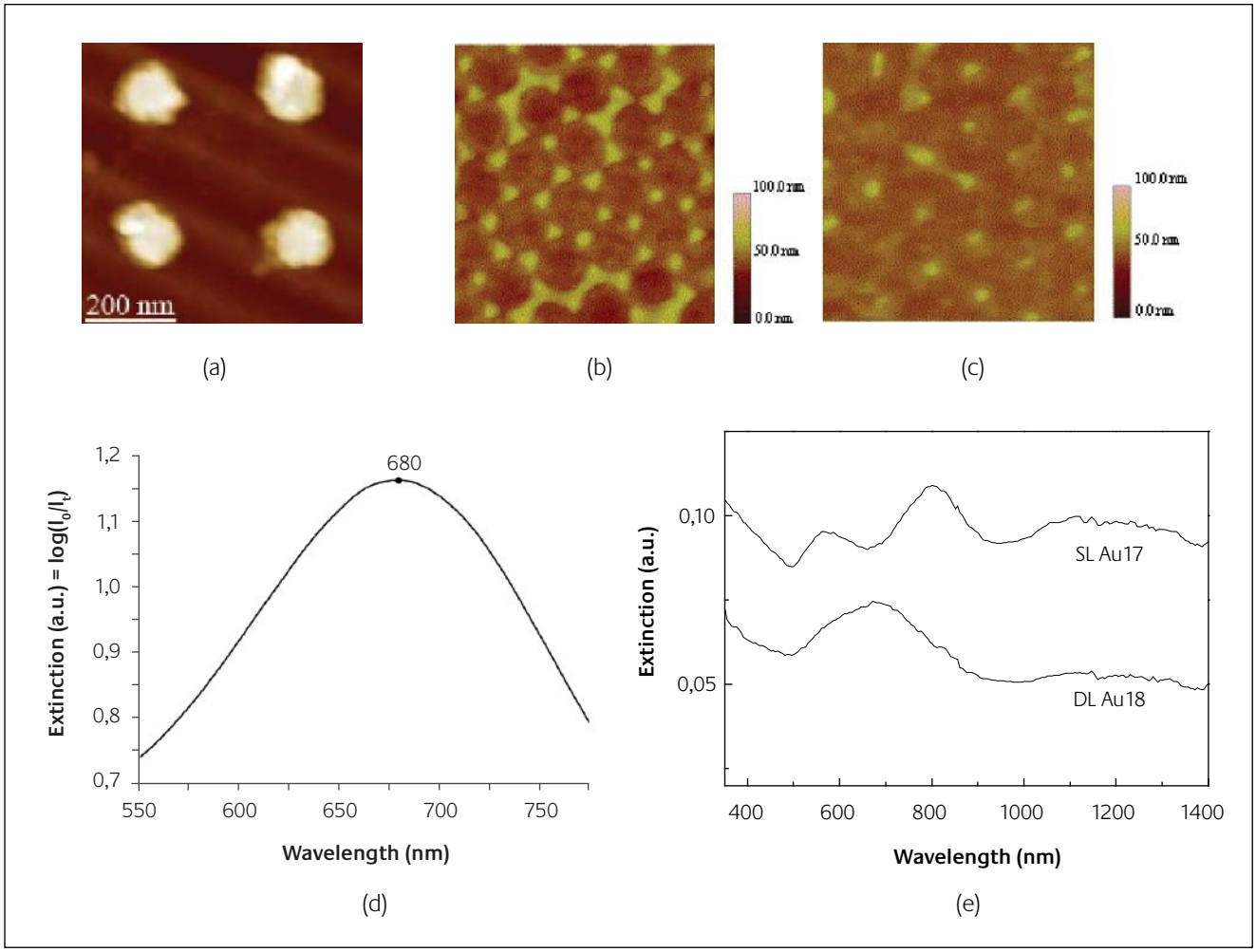

Figure 1

AFM images of Au disks arrays fabricated by EBL (a) and NSL using single layer (b) or double layer (c) masks and extinction spectra of Au disks arrays fabricated by EBL (d) and NSL (e) using a single layer (SL Au17) or a double layer (DL 18) mask

by exposing a thin layer of photoresist to high energy electrons. It is followed by a step of chemical development and, finally, by the deposition of the noble metallic film. The process that we used is as following: glass substrates are first cleaned in a freshly prepared piranha solution (3:1 H_2SO_4 (98%), H_2O_2 (30%)) for 30 min. Once cooled, the glass substrates are rinsed abundantly with deionized water and dried with N_2 gas. Then a layer of about 150 nm of poly(methylmethacrylate) (PMMA: 950k) is deposited by spin coating (4000 rpm) on glass substrates and then baked during 20 min at 160°C. Afterwards, an aluminum layer of 10 nm is evaporated on the PMMA in order to make the substrate conductive. The desired pattern is obtained by EBL using a Hitachi S-3500N SEM associated with nanometer pattern generation system (NPGS) from Nabity. The layer of Al is removed using a potash solution (KOH: C = 0.2 M during 30 s). The development of the exposed regions is performed with a mixture of methylisobutylketone (MIBK) and isopropanol (ISO) (1:3 MIBK/ISO) for 60 s. The masks are then rinsed in isopropanol for 10 s. After gold evaporation, a nanodisks array is obtained *via* a lift-off process dipping in acetone during 3h. Examples of an image obtained by Atomic Force Microscopy (AFM) of such arrays and of their extinction spectrum are given in figure 1a and 1d.

Another method of fabrication of metallic nanoparticles arrays is the nanosphere lithography (NSL) (Figure 1). Every NSL structure elaboration begins with the self-assembly of size-monodispersed nanospheres to form a mask [28, 29, 30]. In our case, the mask consisted either in a single or a double-layer of polystyrene (nano) spheres. Briefly, 30 µL of diluted nanosphere solution (1wt% solid, diameter of 200 nm) was dropped onto a cleaned glass substrate that was inclined between 4° and 6° in a chamber with saturated humidity. By controlling the temperature between 35°C and 45°C, homogenous and dense single or double-layers of nanospheres were formed on areas larger than 1 cm^2. After drying, gold films with different thickness were deposited on the substrates at room temperature (RT) using a pulsed laser deposition (PLD) technique. After complete removal of the nanosphere masks by sonication in chloroform, gold nanoparticle arrays with 2D periodic structures were obtained. Figure 1c gives the image of particle arrays fabricated using a single-layer nanosphere mask (SL Au). They show a well-ordered hexagonal array belonging to the p6mm plane group. Each cell contains 2 triangular-shaped gold particles with a size of 50 nm. Figure 1b exhibits the arrays fabricated using a double layer nanosphere mask (DL Au). The hexagonal array belongs to the same p6mm plane group but each cell contains only one particle with a smaller size compared to SL arrays. The shape of the particles should be consistent with that of the interstices let by the polystyrene nanospheres *i.e.* triangular and hexagonal for SL Au and DL Au arrays respectively. In fact, the particle shape was smoothed slightly during the fabrication process as evidenced in the AFM images so that, in the case of DL Au arrays, the particles appear almost circular. Two resonance peaks are observed for SL Au arrays in the range [400-1000 nm] whereas only one (broad) peak is observed for DL Au arrays. This behavior can be explained by the difference in shape between the individual particles obtained in both cases. For SL arrays, the particles are generally highly anisotropic (typically a height of 17 nm and a diameter of 50 nm) so that the different geometrical depolarization factors found in- and out-of-plane lead to two separate resonances. For DL arrays, the shape of the particles is smoother and only slightly anisotropic so that only a broad peak is observed.

2.2 Preparation of thin films by PLD technique

Pulsed laser deposition (PLD) is a thin film deposition technique where a high power pulsed laser beam is focused inside a vacuum chamber to strike a target of the desired composition. Material is then vaporized from the target and deposited as a thin film on a substrate, *i.e.* a silicon wafer, facing the target. This process can occur in ultra high vacuum or in the presence of a background gas.

This technique was first used by Smith and Turner [31] in 1965 for the preparation of semiconductors and dielectric thin films and was applied to high-temperature superconductors in 1987 [32]. Since this pioneering work, the technique has been intensively used for preparing all kinds of oxides, nitrides, carbides, metallic systems and even polymers or fullerenes. The metal films used in our work (Au, Ag, AuAg) were prepared on quartz substrate in vacuum (~10 Pa) from a foil of metal (purity 99.99%, diameter 40 mm) at a distance of about 40 mm. A XeCl excimer laser [308 nm, 17 ns full width at half maximum] operating at 1 Hz was used.

Although many experimental conditions influence the properties of metal films, we have only investigated two main factors to tune the properties of metal films, *i.e.* the film thickness and the substrate temperature during deposition. We found that the metal film can change from a cluster-like material to a bulk-like one when the thickness increases, the surface plasmon resonance (SPR) band being red-shifted before disappearing. Also, the film can change from a bulk-like material to a cluster-like one with the increase of the deposition substrate temperature.

3 A plasmonic application of gold nanostructures: multimodal detection [33]

In one of our papers [33], we have proposed to use luminescent hybrid nanoparticles initially developed for *in vivo* multimodal imaging [34] to detect the biotin/streptavidin binding by a double detection: a shift of the localized surface plasmon resonance of an array of gold nanodisks and the luminescence of the nanoparticles (gadolinium oxide cores encapsulated in polysiloxane shells containing rhodamine). EBL was used to fabricate square arrays of gold nanodots each dot having a mean diameter of 140 nm and a mean height of 70 nm. The LSPR associated presents a very slight overlap with the dye emission ($\lambda_{emission}$ [Rhodamine] ~590 nm) avoiding thus a strong luminescence quenching of the dyes. We prepared two types of samples differing by the centre to centre distance

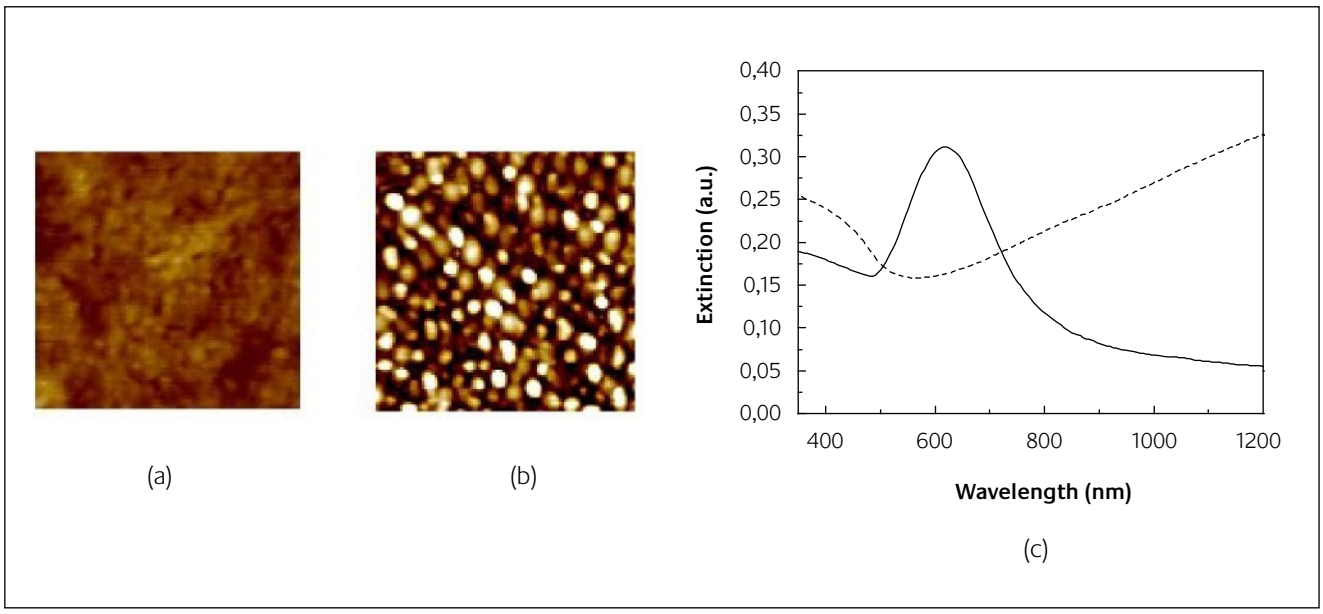

Figure 2

AFM images (area of 500 x 500 nm^2) of "bulk-like" Au (a) films prepared at room temperature and "cluster-like" Au (b) films prepared at high temperature (600°C). (c) Extinction spectra of flat (dashed line: (a)) and rough (solid line: (b)) Au films

between nanoparticles. Gold dots separated by 1140 nm were used for luminescence imaging of hybrid nanoparticles. Gold dots separated by 340 nm were used for LSPR measurements Table 1 gives the mean diameter and the mean height of nanoparticles checked by Atomic Force Microscopy (AFM).

The luminescent core-shell particles which consist of a gadolinium oxide core encapsulated in a polysiloxane shell containing rhodamine are fabricated in two steps. In the first step, gadolinium oxide particles were precipitated by applying a modified 'polyol' protocol [35, 36]. In the second step, a polysiloxane shell is deposited on the gadolinium oxide cores by hydrolysis/condensation of a mixture tetraethylorthosilicate (TEOS), (3-aminopropyl)triethoxysilane (APTES) and rhodamine B isothiocyanate coupled to APTES (APTES-RBTIC) [37],[38]. This allows both the encapsulation of the dyes (RBTIC) within the shell and the presence of amino groups which act as anchoring sites for streptavidin functionalization. The size of the core-shell was 5.0 ± 0.2 nm and the quantity of streptavidin was adjusted in order to obtain, under the assumption of a 100% yield, a functionalization ratio of one streptavidin per particle. The solution then contains $7{,}5.10^{-7}$M of core/shell particles and $7{,}5.10^{-7}$M of streptavidin.

Table 1

Dimensions of Au disks before and after the functionalization of luminescent nanoparticles (NP)

Lattice parameter (nm)	Height (nm)		Diameter (nm)	
	Au	Au±NP	Au	Au±NP
340	70±2	77±2	143±2	159±2
1140	71±2	78±2	140±2	155±2

Table 1 gives the dimensions of the gold dots before and after the functionalization of core-shell particles. It proves that the gold dots are effectively coated by the core/shell particles. Indeed, the height increases from 70 nm to 77 nm by a value of 7 nm, which is the order of magnitude of the average size of the deposited particle (5 nm). In parallel, the diameter increases by approximatively twice this value (15 nm). That the height or half-diameter increase (7-8 ± 1.5 nm) does not exactly match the particle size (5 nm) can be easily understood by the fact that the particle is not in close contact with the gold disks but separated from them by a streptavidin molecule (total length: 6 nm). The height increase does not coincide either with the sum of the particle dimension and the biomolecule size. This implies that during AFM observations the particles should be slightly displaced under the tip. Such displacements are certainly due to the flexibility of the organic binding between surface and particles. They also indicate that, for the concentrations used during immersion of substrates in particles solution, the particles paving on gold dots is certainly not compact. This will be verified by further investigations.

3.1 Detection by shift of localized surface plasmon resonance

For a complete evaluation of the particles ability to evidence the biotin/streptavidin binding, the position evolution of the LSPR of the substrate was measured at all the different steps of the process. Before chemical modification, the gold array is characterised by a LSPR wavelength at λ_{LSPR} = 680 nm (Figure 3: red curve). After the first chemical treatment aiming at deposing a covering biotin layer on gold, the extinction spectrum undergoes a slight red-shift of 3 nm (Figure 3: blue curve). Such a shift which confirms the presence of the biotinylated fixing layer is in good

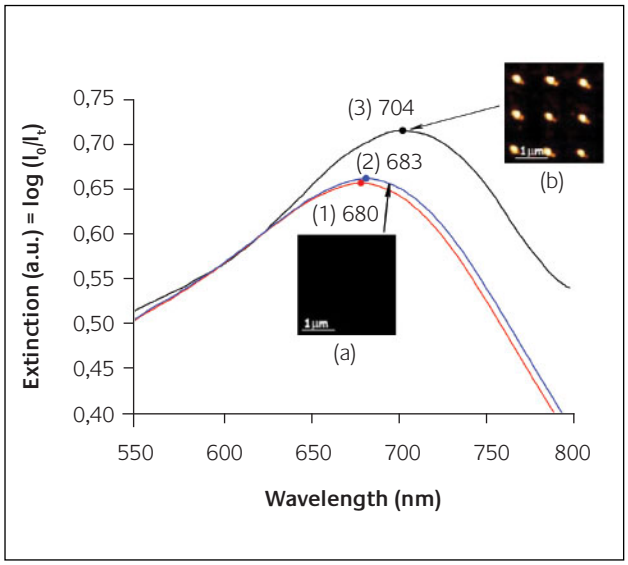

Figure 3

Smoothed extinction spectra: (1) Au disks before chemical modification, (2) Au disks after adsorption of biotin and (3) Au disks after the functionalization of nanoparticles labelled SA ([SA]=7.5x10^{-7}M). With the SNOM images inset corresponding to steps of before (a) and after (b) the incubation of biotinylated Au disks with streptavidin conjugated nanoparticles

agreement with that already measured in previous work [10].

The next step consisted to bind particles labelled streptavidin to the gold dots so biotinylated. The LSPR wavelength was then measured and a λ_{LSPR} value of 704 nm was found. Consequently the shift was of 21 nm compared to the biotinylated Au without nanoparticles (Figure 3).

This shift is due to a local change refractive index or effective thickness of the layer [10,33]:

$$\Delta\lambda = m\Delta n\,[1-\exp(-2d/l_d)] \qquad (1)$$

where $\Delta\lambda$ is the shift of LSPR wavelength, m is the sensitivity of gold dots to the local refractive index, Δn is the local change of refractive index induced by adsorbate ($\Delta n = n_{adsorbate} - n_{air}$), *d* is the effective adsorbate layer thickness and l_d is the characteristic evanescent electric field decay length. The value of sensitivity is 200 nm/RIU (Refractive Index Unit) [10-11] according to our experiments. The value of l_d, which was performed by the Finite Difference Time Domain (FDTD) calculations and Prony's method [39], is equal to 27 nm. The effective thickness of the particles deposited can then be deduced from the wavelength shift $\Delta\lambda$ = 21 nm and the refractive index change Δn = 0.53. *d* is equal to 3 nm. When comparing this value to the size of the particles (5 nm) and that of the streptavidin/biotin couple (6 nm), it can be concluded that the paving density is 0.27. Compared to the maximal density obtained in the case of the hexagonal paving (0.90), the paving density of nanoparticles is 30% of the maximal one for the incubation concentration used here ([SA] = 7.5x10^{-7} M).

3.2 Detection by SNOM images

After having demonstrated that particles could be successfully used for detecting the streptavidin/biotin specific binding by measuring the LSPR shift that they induce on a real probed zone of 30x30µm^2, the next step is now to validate the SNOM technique as an additional route to detect the same interaction. When recording the substrate functionalized by the particles encapsulating RBTIC on a zone of ~3x3 µm^2, we obtained the image of figure 3b (to be compared to that of Figure 3a without particles). They clearly evidence that RBITC which is present on the substrate is strongly localized on the gold dots. Indeed, the spots form a lattice quite similar to that of the dots. The size of the spot (200 nm) is also in good agreement with the size of the coated dots at their basis (200 nm) a value slightly larger than that given in Table 1 (160 nm) corresponding to the diameter at middle height. These results confirm the high selectivity of the labelling particles already inferred from AFM observations.

In conclusion, our results indicate that the gold arrays elaborated by EBL used in combination with particles encapsulating dyes are good candidates for increasing the reliability of biological detection. Indeed they constitute the bases for new devices permitting two types of detection techniques. In a near future, we will extend the study to various molecules like DNA or peptide nucleic acids.

4 Surface-enhanced chemiluminescence (SECL) [24], [40], [41], [42], [43] Demonstration of SECL [24]

Gold films prepared by PLD technique from 30 to 700°C were used to study SECL. As shown in AFM images (Figures 2a and 2b) and Table 2, flat and smooth films are obtained when the substrate is maintained at room temperature whereas corrugated surfaces are obtained for temperatures higher than 200°C. According to Figure 2c, the flat films exhibit the mean features of the extinction of gold bulk [44], whereas for heating at temperatures higher than 200°C the films present a pronounced SPR extinction peak characteristic of the presence of clusters [45]. This peak is located at about 600 nm and presents a blue shift with increasing the temperature of the substrate (Table 2).

Table 2

Characteristics of the samples elaborated by PLD

	Temperature (°C)	SPR position (nm)	SPR intensity	Roughness (nm)	Particle size (nm)
	30	No peak	No peak	0.3	-
	200	670	0.23	1.3	~15
	300	635	0.21	1.5	~20
Au film	400	625	0.37	1.5	~25
	500	625	0.40	1.6	~30
	600	620	0.42	1.9	~35
	700	610	0.43	2.0	~50

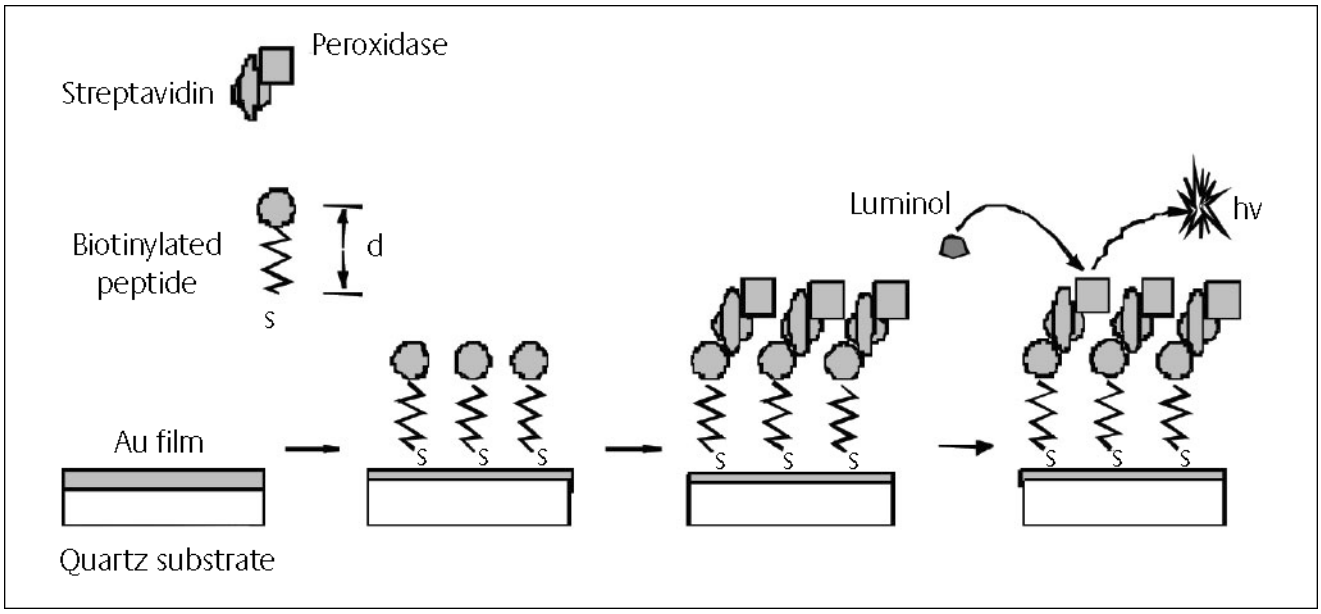

Figure 4

Schematic processes of SECL experiments

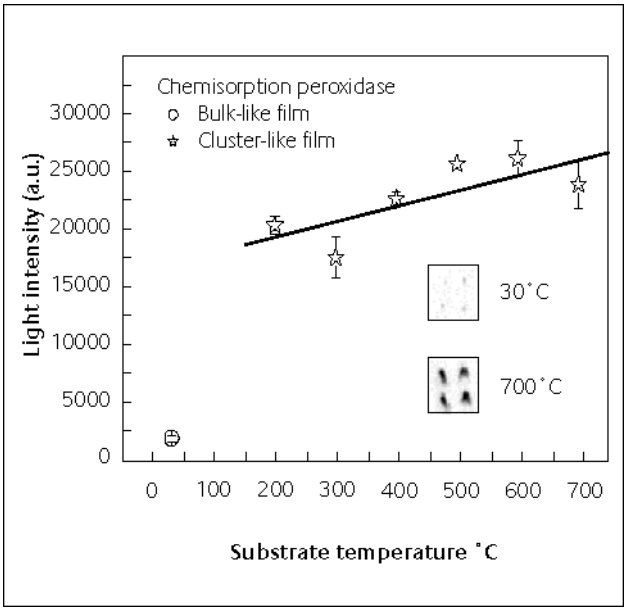

Figure 5

Chemiluminescence intensity induced by peroxidase labeled molecules physisorbed on substrates made at different temperatures: 30, 200,300, 400, 500, 600, and 700°C. Insets: chemiluminescence spots for substrates made at RT and 700°C, respectively

After elaboration of the substrates, luminol CL can be generated at their vicinity following a process described in Figure 4. Firstly, tri-thiolated polypeptides containing 11 amino-acid and modified with a biotin molecule at their N-term end were spotted as 1.2 nl drops (1 mg/ml) on the Au thin films through an automatic piezoelectric spotter (BCA1, Perkin Elmer). The peptides were incubated during 2 hours and then washed to remove all unbound molecules. In a second step, the treated films were immersed for 20 minutes in VBS containing additional 1% bovin serum albumin (BSA) and 0.1% polyoxyethylenesorbitan monolaurate (tween) and finally incubated with peroxidase labelled streptavidin (1 µg/ml) for 30 minutes. The CL measurements were taken with a −30°C cooled CCD camera (Intelligent Dark Box II, Fuji Film). After immobilization of labelled streptavidin, the samples were dipped into a VBS solution containing luminol and additives agents favoring its CL (220 µM luminol, 500 µM H_2O_2 and 200 µM p-iodophenol). The light emitted by the luminol brought at peroxidase vicinity was integrated for 10 sec. The images obtained were quantified and the results were given in arbitrary units (a.u.) and each value was an average of four measurements.

Figure 5 which displays the CL intensity near Au thin films clearly demonstrates that a net enhancement is induced by films corrugation. Indeed, the luminescence is considerably stronger for the films which present the optical properties characteristic of clustered samples (those made at substrate temperatures higher than 200°C). For instance, the intensity of the luminescence emitted by luminol is around 1700 at vicinity of the flat bulk like film prepared at 30°C, whereas it is comprised between 17 000 and 26 000 near the corrugated films prepared above 200°C. Inset in Figure 5 also illustrates this phenomenon: the images of the CL spots are more clearly visible when the substrate is corrugated (preparation at 700°C) than when it is flat (preparation at RT=30°C).

Influence of the distance between substrate and peroxidase [40]

A few influencing factors were studied to understand the effect of SECL, among them the distance to metal substrate, the substrate morphology and the pH. To evaluate the effect of the distance between the emitting luminol and the substrate, different peptides differing from their chain length were used. Precisely, peptides containing 5, 11, 17, or 23 amino acids (denoted respectively as P5, P11, P17 and P23) and having a length, d, of about 1.3, 3.5, 5.7 and 7.8 nm

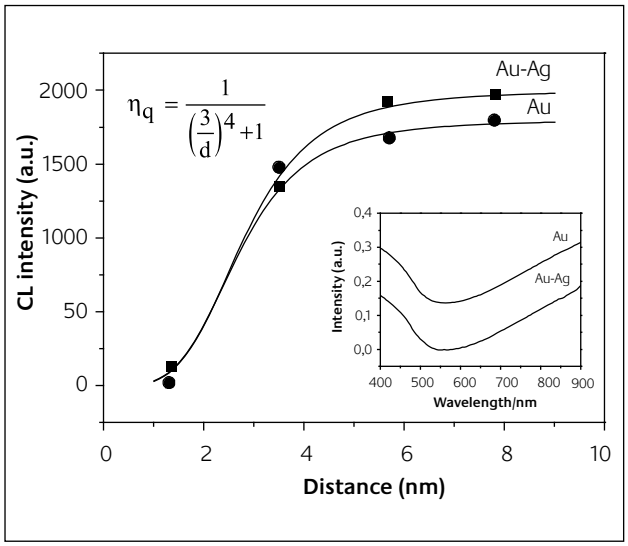

Figure 6

Luminol-H_2O_2 chemiluminescence induced by peroxidase on (flat) bulk-like Au (circles) and Au–Ag films (squares) with different metal/peroxidase distances. The lines are fits of these data according to a Förster process simulation. Insert: absorption spectra of the flat films

were spotted to get different separation distances between substrate and peroxidase.

Figure 6 shows the results of luminol CL near bulk-like Au and AuAg films respectively. In both cases, the CL intensity increases with the distance and reaches about 2,000 in arbitrary units (a.u). Assuming that in absence of clusters, there is no catalytic effect, this increase should be entirely related to the decrease in metal quenching with the distance. Förster transfer theory predicts that such a quenching possesses an inverse fourth power dependence with the distance d^{d-a} between donor and acceptor:

$$\eta_q \approx \left(1 + \left(d_0^{d-a} / d^{d-a}\right)^4\right)^{-1}$$

[46]. In this relation d_0^{d-a} is a critical distance between donor and acceptor and

$$\eta_q = I / I_0$$

is the ratio of dye fluorescence in presence of a film at the distance d^{d-a}, I, and that in absence of the film, I_0. Figure 6 shows that in the case of both Au and Au-Ag flat bulk-like films, such a relation is satisfied between the fluorescence intensity *I* and the distance *d* between the film and the catalyzing peroxidase. A same fit

$$\eta_q = \frac{1}{\left(\frac{3}{d}\right)^4 + 1}$$

is effectively obtained for the experimental data relative to both films with *d* expressed in nanometers. The critical value found, d_0^{quench}. = 3±0.5nm for both Au and Au-Ag films indicates then that the critical distance d_0^{d-a} between the film and the luminol is in good agreement with the order of

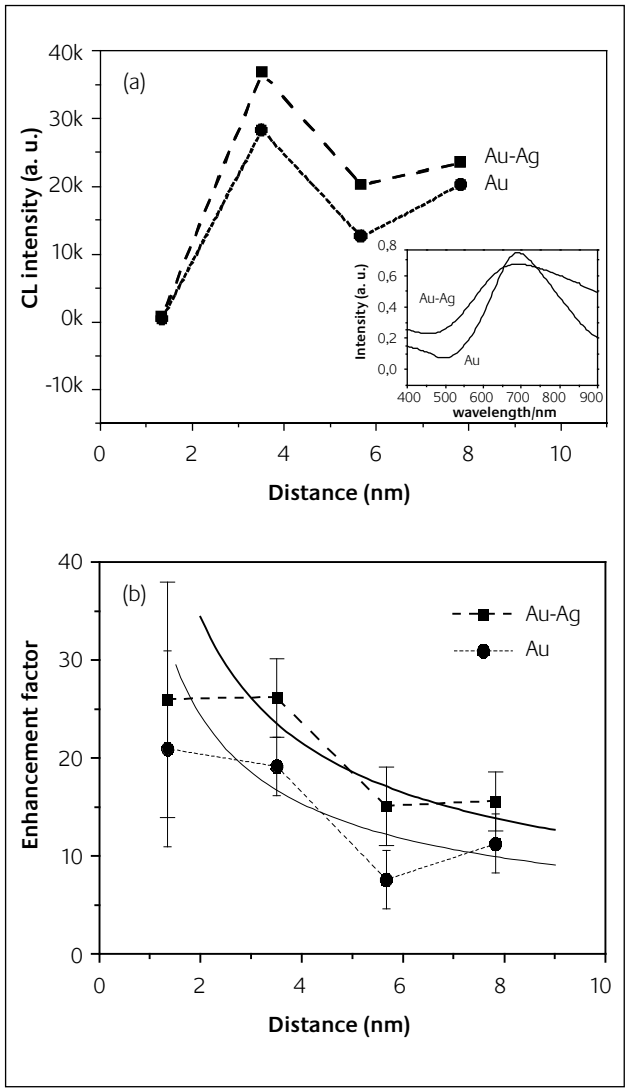

Figure 7

(a) Luminol-H_2O_2 chemiluminescence induced by peroxidase on cluster-like Au (circles) and Au–Ag films (squares) with different metal/peroxidase distances. Insert: absorption spectra of the rough films. (b) Enhancement factor: experimental data (symbols) and data fit (line). The dash lines are guides for the eye

magnitude given by Förster for the critical donor/acceptor distance, between 5 and 10 nm. For distances *d* larger than 6 nm, the fluorescence reaches a plateau at a value which is independent of the chemical nature of the film (1800 for Au and 2000 for Au-Ag).

Completely different is the CL signal near cluster-like Au or Ag films. Indeed, Figure 7 shows that the CL intensity first strongly increases with the distance between 1.3 nm to 3.5 nm and then slowly decreases after 3.5 nm. For a peroxidase/metal distance of 3.5 nm (P11) the intensity reaches high values around 30,000 in the same arbitrary units. As evidenced previously, this increase of more than one order of magnitude compared to the CL intensity near flat films (Figure 6) must be attributed to an enhancement of the fluorescence by the presence of clusters. To provide a quantitative information upon this enhancement, a simple model in which the intensity observed is the product of the quenching factor η_q (≤1) and an enhancement one η_e (≥1) can be proposed: $I = \eta_q \eta_e I_0$.

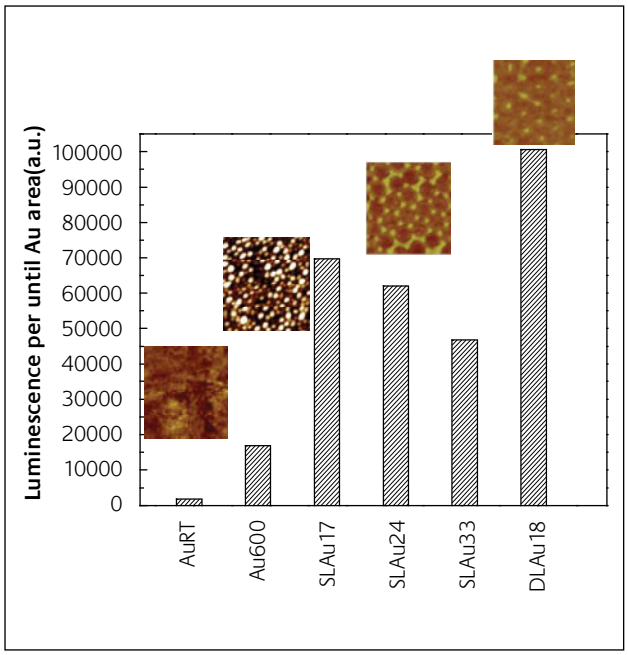

Figure 8

Chemiluminescence intensity per unit area of Au on the flat and corrugated film and nanoparticle arrays

The enhancement factor η_e (Figure 7b) can thus be derived from the relation: $\eta_e = I/\eta_q I_0$, where I is given in Figure 7a and $\eta_q I_0$ in Figure 6.

As expected, the η_e evolution is found to decrease with the distance. However, the decreasing trend is smoother than that relative to quenching. Indeed, when fitting η_e according to a relation similar to that relative to

$$\eta_e = 1 + \left(\frac{d_0^{enhanc.}}{d}\right)^n$$

where n is an integer and $d_0^{enhanc.}$ is a critical distance for enhancement, one finds that $d_0^{enhanc.}$ is much smaller than 4 the exponent related to quenching and that $d_0^{enhanc.}$ is much larger than $d_0^{quench.} \approx 3$ nm.

Precisely, $\eta_e = 1 + \left(\frac{230}{d}\right)^{0.7}$ for $\eta_e = 1 + \left(\frac{350}{d}\right)^{0.7}$ for AuAg with *d* expressed in nm.

The relative variations of quenching and enhancement explain the particular behavior of CL intensity with distance observed in Figure 7a. At short distance, quenching predominates so that CL is low, whereas when increasing the distance, the enhancing mechanism dominates. That explains the presence of a maximum at a distance of 3.5 nm (for P11) slightly larger than d_0^{quench}.

Influence of the morphology of gold film [41]

To evaluate the influence of the corrugation of the films upon SECL, different morphologies summarized in Table 3 were investigated: flat films elaborated by PLD at RT, films with random roughness elaborated by PLD at 600°C and films with a controlled roughness elaborated by NSL using single and double layers masks. In all cases, a polypeptide with a chain length of 7.8 nm (P23) was used to separate the peroxidase from the Au surface.

To evidence an eventual effect of the nature of corrugation upon luminol CL, this latter must be normalized by the effective gold surface area which strongly differs between the randomly corrugated films (for which gold covers all the substrate surface) and the particles arrays (for which gold only lies in small and isolated islands). Figure 8 shows that the area-normalized luminescence is of almost one order of magnitude higher in the case of the particles arrays than for randomly corrugated films which is an indication that the roughness morphology is a key parameter for CL enhancement.

A particle-mediated transfer [23] in which the electrons at vicinity of highly curved surface are the ones which cause some electron transfer from gold clusters to adsorbed H_2O_2 and permits to produce the key intermediate hydroxy and hydroperoxide radicals has already been proposed to explain the enhancement of CL in the case of particles [47]. The authors showed that the transfer was favoured for particles sizes comprised between 20 and 40 nm. Applied to

Table 3

Characteristics of the films elaborated

	Samples	In-plane particle size (nm)	Out-of-plane particle height (nm)	SPR peak (nm)	CL intensity (a.u.)	Au surface ratio (%)
Nanoparticle Arrays	SL Au17	50	17	565-802	17800	25.5
	SL Au24	50	24	583-715	20300	32.7
	SL Au33	50	33	620-722	19700	42
	DL Au18	30	18	667	8860	8.8
Flat Au film	Au RT	/	25	No peak	1800	100

'Au surface ratio' denotes the gold area normalized to that of supporting glass

corrugated films this indicates that the ideal roughness permitting to obtain a large plasmon resonance should be characterized by curvature radii half of this particle diameter: *i.e.* in the [10-20 nm] range. The randomly corrugated film which possesses a roughness of 2 nm is characterized by curvature radii of a few nanometers at particles junction. These curvatures are then too small to induce a large CL enhancement. On the contrary, the dots top of the particles arrays dots are characterized by curvature radii that are approximately half of the particles in-plane diameter given in Table 3 (25 nm for SL arrays, 15 nm for DL arrays) and then lie in the ideal range inducing the maximal enhancement (15 nm).

Influence of the pH value [42]

Among the factors influencing the reactive conditions between luminol and hydrogen peroxide, pH, which is involved in the light emitting steps of luminol oxidation, was found to be one of the more important [48]. In order to study the influence of pH value, a biotinylated peptide with a length sufficiently small, 3.5 nm, (P11) to ensure a significant catalytic effect without correlative light emission quenching by metal, In the process of CL measurement, the films were divided in eight compartments separated by a hydrophobic layer and the pH of each compartment was adjusted to values varying from 7 to 12 (7, 8, 8.5, 9, 10, 11, 11.5, 12) by addition of suitable quantities of NaOH (5N) or HCl (6N).

The reaction of luminol/H_2O_2 catalysed by peroxidase involves two principal stages: (i) the first one is the enzymatic stage appearing as the sequence of the following reactions (R) [49]:

$$P+H_2O_2 \rightarrow PI+H_2O$$
$$PI+L \rightarrow PII+L^{\bullet -}$$
$$PII+L \rightarrow P+L^{\bullet -}+H_2O$$

where P, PI, and PII are peroxidase and two intermediate complexes respectively; L and $L^{\bullet -}$ are luminol and the product of free-radical single-electron oxidation respectively. (ii) The second stage involves the transformation from $L^{\bullet -}$ to 3-aminophthalate in an excited state which results in light emission [50]. In presence of peroxidase [51], luminol CL is maximal for pH ranging between 8 and 9 whereas in absence of this catalyst [52,53], the maximum of CL locates at 10-11 pH value.

The influence of pH upon luminol/hydrogen peroxide CL was first investigated for reactions occurring near flat surfaces. Figure 9 which displays the CL intensity as a function of pH on flat glass, Au and Ag films clearly shows two different types of behaviour for, on one hand, the glass support and, on the other hand, the metal films. For glass, CL is maximal for pH comprised between 8.5 and 9 and is almost equal to zero for pH superior to 10. This indicates that at vicinity of glass, peroxidase acts effectively as a catalyst for the reactions responsible for luminol CL. This result is in agreement with

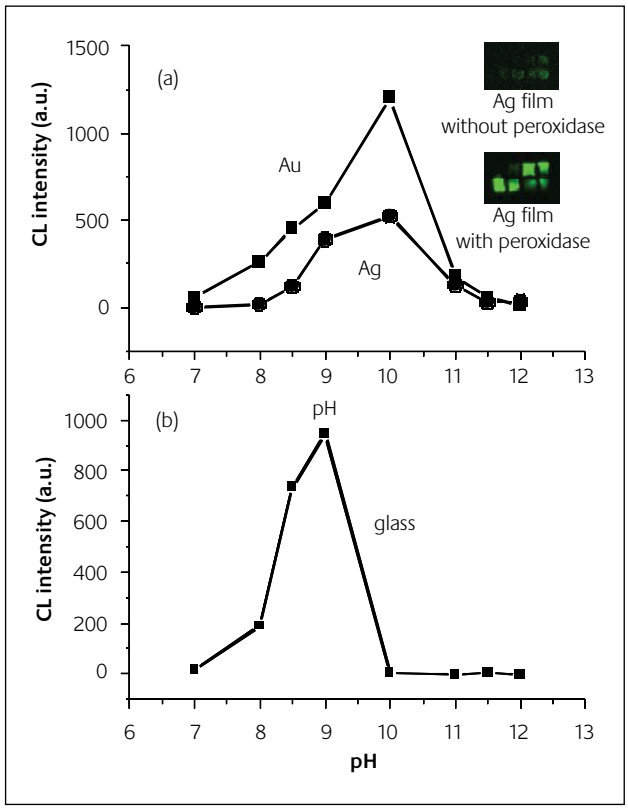

Figure 9

Effect of pH upon the chemiluminescence of the luminol-H_2O_2 system catalyzed by peroxidase at vicinity of Au and Ag films (a) and flat glass (b). Inset CL at different pH on flat Ag films in presence or in absence of peroxidase; from left to right, pH in first row corresponds to 7, 8, 8.5 and 9 and in second row to 10, 11, 11.5 and 12

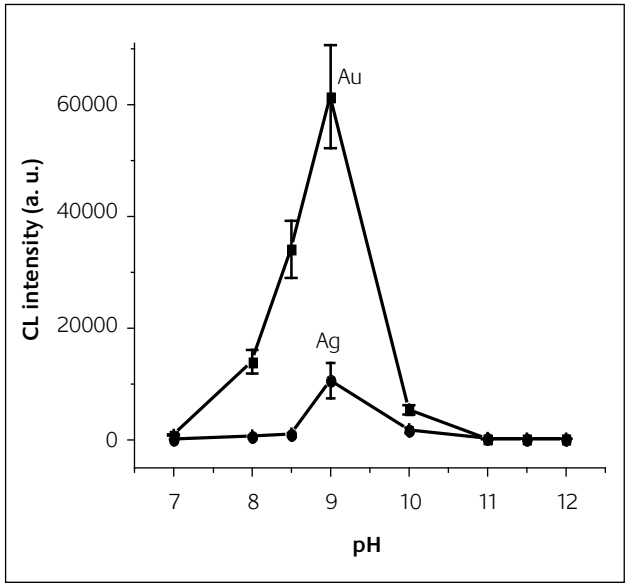

Figure 10

Effect of pH upon the chemiluminescence of the luminol-H_2O_2 system catalyzed by peroxidase at vicinity of corrugated (cluster-like) Au and Ag films. Corrugation induces an enhancement of the chemiluminescence at pH 9

the fact that peroxidase was already found to catalyze CL at vicinity of glassy carbon electrodes [51]. On the contrary, in the case of Ag and Au, CL is low at pH 8.5 and is maximal in the pH range comprised between 9 and 11. This indicates

that the catalytical activity of peroxidase is strongly decreased when the enzyme is fixed on flat metal film which is probably due to a light emission quenching not yet negligible at a distance of around 10 nm from the metal.

Figure 10 gives the CL intensity as a function of pH on *cluster-like* Au and Ag films. The first observation is that, for both metals, CL is systematically greater than in the case of flat films. This shows that nano-corrugation induces a significant CL enhancement at all the pH values studied and not only at pH 8.5 (the pH fixed in previous experiments). Moreover whereas CL presents a maximum at pH 9 for both metals, the signal is much more important for nano-corrugated gold which indicates clearly that it is a better catalyst than corrugated silver. Concerning silver, very striking is that the position of the CL maximum depends on the morphology of the film: whereas in absence of corrugation, CL is maximal at around pH 10 (a range favouring the reactions taking place without help of peroxidase), it is maximal at pH 9 in presence of corrugation. Since pH 9 increases peroxidase activity, this could prove that corrugation enhances preferentially the reactions involving the enzyme. This conclusion is reinforced by the case of gold for which the maximal CL observed is also shifted in the exact range of pH (8.5 – 9) favouring peroxidase-related reactions. In absence of peroxidase, Zhang *et al*. found that gold particles significantly enhance CL of the luminol-H_2O_2 system at pH 12 [23]. They suggest that the O-O bond of H_2O_2 is broken up into double $OH^{\bullet}$ radicals by virtue of gold catalysis facilitating then the formation of luminol radical $L^{\bullet -}$. Our present experiments confirm this result since at pH 12 (a pH at which peroxidase does not act as a catalyst) they also evidence a CL enhancement induced by corrugation. Indeed luminol CL increases of around one order of magnitude from 10±3 in arbitrary units at vicinity of flat gold (Figure 9) up to 130±40 near corrugated gold (Figure 10). However, when peroxidase is grafted on corrugated gold, luminol CL is maximal at pH 9 (the pH enhancing catalysis by peroxidase) and strongly greater than at pH 12: 61300 instead of 130 in the same arbitrary units. The reactions involving peroxidase are then also surface-enhanced but with an enhancement factor of two orders of magnitude (at pH 9, CL increases from 600 at vicinity of flat gold up to 61300 near corrugated gold).

Catalytical mechanism of SECL [43]

To definitely prove that SECL is related to a catalytic effect, three chemically different samples (Au, Ag, AuAg alloys) having their plasmon absorption peaking at the same energy (620 nm) were studied (Figure 11b). The 620 nm position lies far from luminol emission (425 nm) so that the low overlap resulting between SPR and dye luminescence should limit plasmon assistance to CL enhancement. Then if strong

Table 4

Characteristics of the samples studied

	T (°C)	SPR position (nm)	Roughness (nm)	Particle size (nm)	Peptide density (peptide/nm²)
Au	600	620	1.9	~35	1.6 ± 0.5
AuAg	200	620	4.0	27	2.5 ± 0.7
Ag on $BaTiO_3$	600	620	3.6	37	3.2 ± 0.9

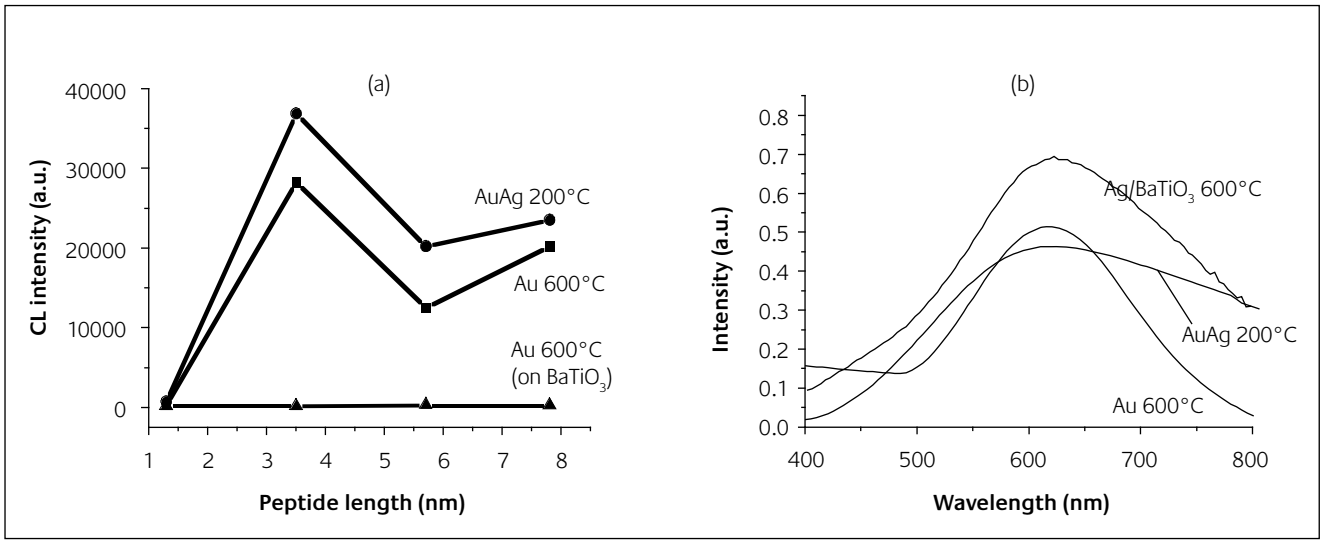

Figure 11

(a) luminol-H_2O_2 CL induced by peroxidase on cluster-like Au, Ag and Au-Ag films prepared at different temperatures with different metal/peroxidase distances. (b) extinction spectra of Au, Ag and AuAg films

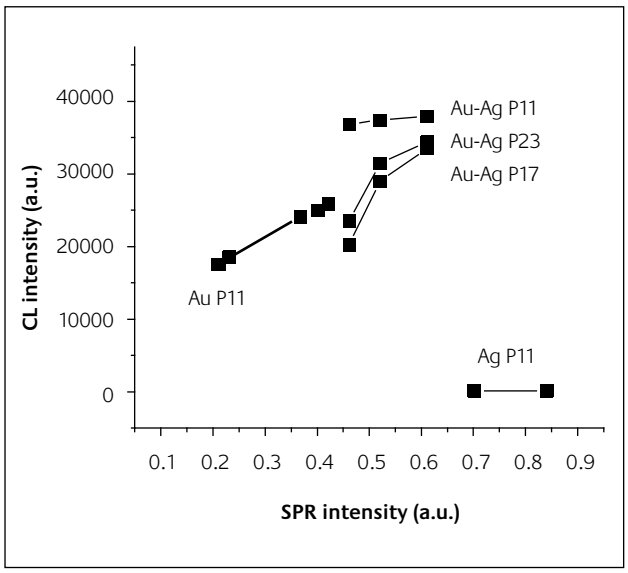

Figure 12

Relationship between the CL and SPR for metal families that differ in their composition: Au, Ag and AuAg alloys. Within a same family the different points correspond to different corrugations (and for Au to different peptide grafting)

differences were evidenced in CL between all the metals investigated, it should be concluded that SECL clearly originates from catalytic mechanisms. All the characteristics of the samples studied are indicated in Table 4 including the density of polypeptide (P11) grafting.

The behavior of luminol CL at vicinity of cluster-like Ag films completely differs from that observed at vicinity of Au or AuAg ones (Figure 11a). Whereas corrugation leads to an enhancement of more than one order of magnitude for Au and AuAg, it leads to only an increase comprised between 50 and 100% for Ag. This (relatively) low increase is consistent with that already reported by Aslan *et al*. who studied differently coloured CL reagents [54]. The difference in the enhancement cannot be attributed to a deficit in the peptide densities of Ag substrates since the amount of polypeptides grafted is greater for silver than for gold. It definitely then indicates that other mechanisms than plasmon-assisted processes should be involved in SECL and as stated by Zhang *et al*. [23], the nature of the main mechanisms responsible for SECL should be catalytic.

CL is consecutive to luminol oxidation into a luminol radical. Two main mechanisms for catalysing this oxidation can be proposed. The first mechanism can be inferred from the apparent contradiction that catalysis involves contact interaction occurring at distances up to 1 nm whereas the CL enhancement is evidenced here for metal/peroxidase distance largely greater (around 5 nm). Since the oxidation is known to process in two steps [51] : one involving peroxidase (and then taking place in close contact with it) and the other involving the presence of an oxygen-related radical (and then not necessarily required to append at close vicinity of peroxidase), this is this latter step which is most certainly catalysed by the presence of corrugated gold [55]. According to the reactions (R), the catalytic mechanisms involving peroxidase require the presence of hydrogen peroxide. It is then possible that metal catalysis could arise from an enhanced electron transfer from metal clusters to adsorbed H_2O_2. This particle-mediated transfer [56], permits to produce some key radicals favouring the formation of complexes containing peroxidase and/or that of luminol radical in presence of these complexes. This interpretation is based on several reports evidencing the formation of active oxygen-containing reactant intermediates such as $OH^{\bullet}$ or when gold particles are used as catalysts [55,57]. The second mechanism, acting in conjunction with the first one, could arise from a decrease of the redox potential of luminol at vicinity of corrugated gold. Such a shift which facilitates luminol oxidation in presence of catalysing peroxidase was already evidenced by our team when luminol is directly fixed on gold cluster [58]. In any case, the catalytic enhancement arises from the modification of thermodynamic properties at vicinity of highly curved surfaces [59] and is expected to increase with roughness for all the metals investigated here. This correlation was already observed in the case of gold cluster [23] for which CL increases by 25% when roughness increases from 1.3 to 1.9 nm. We also verified it for AuAg alloys for which CL increases of more than 50% for a roughness increase from 4.0 to 4.4 nm and even for Ag for which an increase of roughness from 3.1 to 3.6 nm leading to a CL increase of around 30%.

A correlation between SPR intensity and CL enhancement has already been pointed out in literature [23]. Figure 12 which summarizes all the results that we have obtained shows that, in fact, such correlations can be found within each metal family (Au, Ag or Au/Ag) but cannot lead to an universal rule that would be valid regardless the nature of the metal. The reason for which such a correlation can be established within each kind of metal is that SPR intensity and SECL have a similar evolution with roughness. Roughness increases the number of localized electrons responsible for strong Mie resonances. It increases also the film curvatures responsible for an increased catalytic activity. Then, whereas LSPR intensity is an indicator of the number of metal electrons liable to catalyse CL [60], the efficiency of the catalysis depends on the chemical nature of the metal.

5 Conclusions

In this paper, we have demonstrated that both plasmonic and catalytic properties of corrugated gold could lead to new applications in the field of biological detection. In the first part, we have shown how the plasmonic properties could allow the detection of the biotin-streptavidin binding by two types of techniques: extinction spectroscopy and luminescence microscopy when the probe (here the streptavidin) is labelled by luminescent particles. In the second part, we have demonstrated that the catalytical properties of gold corrugated surfaces can significantly enhance the chemiluminescence of luminol brought at vicinity.

About the authors

Jean-Louis Bijeon is associate professor at University of Technology of Troyes, he is the Head of the Physics, Mechanics, Materials and Nanotechnology department. He got his PhD from University of Burgundy (France) and from Oak Ridge National Laboratory (USA) in 1989 on Surface Enhanced Raman Scattering and its relations with the Localized Surface Plasmon Resonance on submicronic metallic particles. He was the R&D project manager, in scanning tunnelling microscopy and photon scanning tunnelling microscopy at SPIRAL R&D a French private company, from January 1990 to February 1994. Now its research themes inside the Nanotechnology and Optical Instrumentation Laboratory at UTT, are near-field optics and related fields involving surface plasmon resonance in metallic nanoparticles, and plasmonics. Another field of its activities is the expertise in atomic force microscopy.

Grégory Barbillon completed his PhD in Physics (2007) at the University of Technology of Troyes (France) under the supervision of Prof. J.-L. Bijeon. Then he was awarded a post-doc position at the University of Lyon. In recent years, his interests were focused on plasmonics and these applications in biology and medicine, the nano-optics, the nanofabrication and the luminescence of nanoparticles.

References

1 A.P.F. Turner, *Science*, 2000, **290**, pp. 1315-1317
2 B. Liedberg, C. Nylander and I. Lundstroem, *Sens. Actuators*, 1983, **4**, pp. 299-304
3 L.S. Jung, C.T. Campbell, T.M. Chinowsky, M.N. Mar and S.S. Yee, *Langmuir*, 1998, **14**, pp. 5636-5648
4 L.S. Jung and C.T. Campbell, *J. Phys. Chem. B*, 2000, **104**, pp. 11168-11178
5 L.S. Jung and C.T. Campbell, *Phys. Rev. Lett.*, 2000, **84**, pp. 5164-5167
6 B.L. Frey, C.E. Jordan, S. Kornguth and R.M. Corn, *Anal. Chem.*, 1995, **67**, pp. 4482-4457
7 M. Mrksick, J.R. Grunwell and G.M. Whitesides, *J. Am. Chem. Soc.*, 1995, **117**, pp.12009-12010
8 C.E. Jordan, A.G. Frutos, A.J. Thiel and R.M. Corn, *Anal. Chem.*, 1997, **69**, pp. 4939-4947
9 J.M. Brockman, A.G. Frutos and R.M. Corn, *J. Am. Chem. Soc.*, 1999, **121**, pp. 8044-8051
10 G. Barbillon, J.-L. Bijeon, J. Plain, M. Lamy de la Chapelle, P.-M. Adam and P. Royer, *Gold Bulletin*, 2007, **40** (3), pp. 240-244
11 G. Barbillon, J.-L. Bijeon, J. Plain, M. Lamy de la Chapelle, P.-M. Adam and P. Royer, *Surface Science*, 2007, **601**, pp. 5057-5061
12 G. Barbillon, J.-L. Bijeon, J.-S. Bouillard, J. Plain, M. Lamy de la Chapelle, P.-M. Adam and P. Royer, *Journal of Microscopy*, 2008, **229** (2), pp. 270-274
13 N. Math and A. Chilkoti, *Anal. Chem.*, 2002, **74**, pp. 504-509
14 D. Eck, C.A. Helm, N.J. Wagner and K.A. Vaynberg, *Langmuir*, 2001, **17**, pp. 957-960
15 T. Okamoto, I. Yamaguchi and T. Kobayashi, *Opt. Lett.*, 2000, **25**, pp. 372-374
16 M. Himmelhaus and H. Takei, *Sens. Actuators B*, 2000, **B63**, pp. 24-30
17 H. Takei, *Proc. SPIE-Int. Soc. Opt. Eng.*, 1998, **3515**, pp. 278-283
18 M. Moskovits, *Rev. Mod. Phys.*, 1985, **57**, 783
19 A. Otto, *J. Raman Spectrosc.* 2005, **36**, 97
20 X.M. Dou and Y. Ozaki, *Rev. Anal. Chem.*, 1999, **18**, pp. 285-321
21 K. Sokolov, J. Aaron, B. Hsu, D. Nida, A. Gillenwater, M. Follen, C. MacAulay, K. Adler-Storthz, B. Korgel, M. Descour, R. Pasqualani, W. Arap, W. Lam and R. Richards-Kortum, *Technol. Cancer Research Treatment*, 2003, **2**, pp. 491-504
22 A.A. Ooka and R.L. Garell, *Biopolymers*, 2000, **57**, pp. 92-102
23 Z.F. Zhang, H. Cui, C.Z. Lai, L.J. Liu, *Anal. Chem.*, 2005, **77**, pp. 3324
24 G.W. Lu, B.L. Cheng , H. Shen, Z.H. Chen, G.Z. Yang, C.A. Marquette, L.J. Blum, O. Tillement, S. Roux, G. Ledoux, A. Descamps and P. Perriat, *Appl. Phys. Lett.* , 2006, **88**, 023903
25 W.T. Wallace, R.L. Whetten, *J. Am. Chem. Soc.*, 2002, **124**, pp. 7499
26 R.A.J. O'Hair, G.N. Khairallah, *J. Cluster Sci.*, 2004, **15**, pp. 331
27 L. Prati, M. Rossi, *J. Catal.*, 1998, **176**, pp. 552
28 J.C. Hulteen and R.P. Van Duyne, *J. Vac. Sci. Technol. A, Vac. Surf. Films*, 1995, **13**, pp. 1553-1558
29 A.S. Dimitrov, T. Miwa and K. Nagayama, *Langmuir*, 1999, **15**, pp. 5257-5264
30 U. Ch. Fischer and H.P. Zingsheim, *J. Vac. Sci. Tec.*, 1981, **19**, pp. 881
31 H.M. Smith and A.F. Turner, *Appl. Opt.*, 1965, **4**, pp. 147
32 D. Dijkkamp, T. Venkatesan, X.D. Wu, S.A. Shareen, N. Jiswari, Y.H. Min-Lee, W.L. McLean and M. Croft, *Appl. Phys. Lett.*,1987, **51**, 619
33 G. Barbillon, A.-C. Faure, N. El Kork, P. Moretti, S. Roux, O. Tillement, M.G. Ou, A. Descamps, P. Perriat, A. Vial, J.-L. Bijeon, C.A. Marquette and B. Jacquier, *Nanotechnology*, 2008, **19**, 035705
34 J.L. Bridot, A.C. Faure, S. Laurent, C. Riviere, C. Billotey, B. Hiba, M. Janier, V. Josserand, J.L. Coll, L. Vander Elst, R. Muller, S. Roux, P. Perriat, O. Tillement, *J. Am. Chem. Soc.*, 2007, **129**, pp. 5076-5084
35 R. Bazzi, M. Flores-Gonzales, C. Louis, K. Lebbou, C. Dujardin, A. Brenier, W. Zhang, O. Tillement, E. Bernstein and P. Perriat, *J. Lumin.*, 2003, **102/103**, pp. 445-450
36 R. Bazzi, M.A. Flores, C. Louis, K. Lebbou, W. Zhang, C. Dujardin, S. Roux, B. Mercier, G. Ledoux, E. Bernstein, P. Perriat, O. Tillement, *J. Colloid Interface Sci.*, 2004, **273**, pp. 191-197
37 C. Louis, R. Bazzi, C.A. Marquette, J.-L. Bridot, S. Roux, G. Ledoux, B. Mercier, L. Blum, P. Perriat and O. Tillement, *Chem. Mater.*, 2005, **17**, pp. 1673-1682
38 C. Louis, S. Roux, G. Ledoux, C. Dujardin, O. Tillement, Bo Lin Cheng, P. Perriat, *Chem. Phys. Lett.*, 2006, **429**, pp 157-160
39 D. Barchiesi, T. Grosges and A. Vial, *New J. Phys.*, 2006, **8**, pp. 1-10
40 G. Lu, H. Shen, B. Cheng, Z. Chen, C.A. Marquette, L.J. Blum, O. Tillement, S. Roux, G. Ledoux, M. Ou, P. Perriat, *Appl. Phys. Lett.*, 2006, **89**, 223128
41 H. Shen, G. Lu, M. Ou, C.A. Marquette, G. Ledoux, S. Roux, O. Tillement, P. Perriat, B. Cheng, Z. Chen, *Chem. Phys. Lett.*, 2007, **439**, pp.105-109
42 M. Ou, G. Lu, H. Shen, A. Descamps, C.A. Marquette, L.J. Blum, S. Roux, O. Tillement, B. Cheng, P. Perriat, *Photochemistry and Photobiology* doi: 10.1111/j.1751-1097.2008.00350.x
43 M. Ou, G. Lu, H. Shen, A. Descamps, C.A. Marquette, L.J. Blum, G. Ledoux,

S. Roux, O. Tillement, B. Cheng, P. Perriat, *Adv. Funct. Mater.*, 2007, **17**, pp. 1903-1909
44 G.B. Smith, G.A. Niklasson, J.S.E.M. Svensson and C.G. Granqvist, *J. Appl. Phys.*, 1986, **59**, pp. 571
45 M.C. Daniel and D. Astruc, *Chem. Rev.*, 2004, **104**, pp. 293
46 W.L. Barnes, *J. Mod. Optics*, 1998, **45**, pp. 661
47 A.J. Henglein, *J.Phys. Chem.*, 1993, **97**, pp. 5457
48 H. Cui, Y. Xu and Z.F. Zhang, *Anal. Chem.*, 2004, **76**, pp. 4002-4010
49 I.S. Alpeeva and I.Y. Sakharov, *Appl. Biochem. Microbiol.*, 2007, **43**, pp. 25-28
50 G.H.G. Thorpe, L.J. Kricka, S.R. Moseley and T.P. Whitehead, *Clin.Chem.*, 1985, **31**, pp. 1335-1341
51 C. A. Marquette and L. J. Blum, *Recent Res. Devel. Pure Applied Anal. Chem.*, 2002, **4**, pp. 9-20
52 H. Zhang and H.A. Mottola, *Analyst.*, 1996, **121**, pp. 211-218
53 A. Krasowska, D. Rosiak and K. Szkapiak, *Curr.Top.Bio.*, 2000, **24920**, pp. 89-95
54 K. Aslan, S.N. Malyn, C.D. Geddes, *J. Am. Chem. Soc.*, 2006, **128**, pp. 13372
55 R. Grisel, K.J. Weststrate, A. Gluhoi and B.E. Nieuwenhuys, *Gold Bulletin*, 2002, **35**, pp. 39
56 A. Henglein, *J. Phys. Chem.*, 1993, **97**, pp. 5457-5471
57 S.H. Overbury, L. Ortiz-Soto, H.G. Zhu, B. Lee, M.D. Amiridis and S. Dai, *Catal. Lett.*, 2004, **95**, pp. 99-106
58 S. Roux, B. Garcia, J.L. Bridot, M. Salomé, C. Marquette, L. Lemelle, P. Gillet, L. Blum, P. Perriat, O. Tillement, *Langmuir*, 2005, **21**, pp. 2526
59 J. Gibbs, Collected Works, Yale University Press, New Haven, CT, 1928
60 S. Link, M.A. El-Sayed, *Int. Rev. Phys. Chem.*, 2002, **19**, pp.409